

UC Davis

UC Davis Previously Published Works

Title

Targeting Base Excision Repair Glycosylases with DNA Containing Transition State Mimics Prepared via Click Chemistry

Permalink

<https://escholarship.org/uc/item/21b163zm>

Journal

ACS Chemical Biology, 14(1)

ISSN

1554-8929

Authors

Yuen, Philip K
Green, Sydnee A
Ashby, Jonathan
[et al.](#)

Publication Date

2019-01-18

DOI

10.1021/acscchembio.8b00771

Peer reviewed



HHS Public Access

Author manuscript

ACS Chem Biol. Author manuscript; available in PMC 2020 January 18.

Published in final edited form as:

ACS Chem Biol. 2019 January 18; 14(1): 27–36. doi:10.1021/acscchembio.8b00771.

Targeting Base Excision Repair Glycosylases with DNA containing Transition State Mimics prepared via Click Chemistry

Philip K. Yuen, Sydnee A. Green, Jonathan Ashby, Kori T. Lay, Abhishek Santra, Xi Chen, Martin P. Horvath, Sheila S. David*

Department of Chemistry, University of California, Davis, 95616

School of Biological Sciences, University of Utah, Salt Lake City UT 84112

Abstract

DNA glycosylases of the Base Excision Repair (BER) pathway are front-line defenders in removing compromising modifications of the DNA nucleobases. Aberrantly modified nucleobases mediate genomic mutations and inhibit DNA replication leading to adverse health consequences such as cancer, neurological diseases and aging. In an effort towards developing high-affinity transition state (TS) analogs as chemical biology probes for DNA glycosylases, oligonucleotides containing a propargyl-modified pyrrolidine TS mimic nucleotide were synthesized. A small library of TS-mimic containing oligonucleotides was generated using a structurally diverse set of five azides via copper(I)-catalyzed azide-alkyne cycloaddition (CuAAC) “click” chemistry. The relative affinity (K_d) was evaluated for BER glycosylases *E. coli* MutY (Ec MutY), bacterial formamidopyrimidine glycosylase (Fpg), and human OG glycosylase 1 (hOGG1) with the library of TS-mimic DNA duplexes. All of the BER glycosylases were found to exhibit extremely high affinity ($K_d \sim \text{pM}$) for the TS mimics. However, binding preferences, distinct for each glycosylase, for the TS mimic library members were observed, suggesting different modes of binding and transition state stabilization among the three glycosylases. Fpg bound all of the TS mimics with exceptionally high affinity, while MutY binding affinity correlated inversely with size of the appended moiety. Of note, we identified one member of the small TS mimic library that exhibited particularly high affinity for hOGG1. These results strongly support use of the propargyl-TS mimic oligonucleotides and elaboration via click chemistry in screening and identification of high-affinity ligands for a BER glycosylases of interest.

Introduction

Genomic integrity is constantly threatened by DNA modifications resulting from reactions with endogenous and exogenous agents.¹ The repair of DNA nucleobase modifications is

* Author to whom correspondence should be directed at ssdavid@ucdavis.edu.

Author contributions

P.K.Y. and S.S.D. designed the study. P.K.Y., S.A.G., J.A. and K.T.L. performed the experiments. A.S. and X.C. provided GlcNAcProN₃. M.P.H. performed the modeling studies and generated relevant structural figures. P.K.Y., M.P.H. and S.S.D. wrote the paper with contributions from the other authors. All authors have given approval to the final version of the manuscript.

Supporting Information is available free of charge on the ACS publications website

Supplementary figures and tables, full experimental section and compound characterization

The authors declare no competing financial interest.

initiated by the base excision activity of DNA glycosylases as the first step in the Base Excision Repair (BER) pathway.²⁻⁵ Numerous DNA glycosylases are responsible for removal of a wide array of modified or misplaced DNA bases that result from oxidation, alkylation or polymerase errors.⁴⁻⁶ The DNA oxidation product of guanine, 8-oxo-7,8-dihydroguanine (OG), is removed in bacteria by the Formamidopyrimidine glycosylase (Fpg) and in humans by human OG glycosylase 1 (hOGG1) (Figure 1A).^{2, 4, 7} The presence of OG in DNA is problematic due to its ability to mimic thymine, which can ultimately result in G to T transversion mutations if A is misincorporated opposite of OG during replication.²

Fpg and hOGG1 are bifunctional glycosylases that catalyze OG base excision and associated b-lyase strand cleavage reactions utilizing an amine-containing residue (N-terminal Pro for Fpg; Lys side chain for hOGG1).^{5, 7} Though similar in terms of mechanism and activity towards OG, and several other substrates,^{8, 9} the two glycosylases are from distinct BER superfamilies based on specific structural motifs; hOGG1 belongs to the Endo III/helix-hairpin-helix (HhH) superfamily, while Fpg is a member of the Fpg/Nei helix-two-turn-helix (H2TH) superfamily.^{7, 10} In addition, Fpg exhibits catalytic activity for a much broader array of damaged bases to which hOGG1 has no activity, including several oxidized pyrimidines, and the hydantoin lesions, guanidinohydantoin (Gh) and spiroiminodihydantoin (Sp) (Figure 1A).^{7, 8, 11-13} Somewhat surprisingly, Fpg and hOGG1 are also able to recognize and excise non-polar isosteres of OG indicating that faithful hydrogen-bonding mimicry of the DNA nucleobase is not necessary for activity with these glycosylases.¹⁴ A DNA glycosylase also belonging to the HhH superfamily, MutY/MUTYH (bacteria/human), plays a key role in preventing mutations associated with OG by removing inappropriately inserted A bases from OG:A mismatches.¹⁵ Subsequent processing of the apurinic/aprimidinic (AP) site, and polymerase incorporation of C across from OG provides a second opportunity to completely repair the OG lesion.²

The importance of proper functioning BER enzymes, individually and in tandem, is highlighted by increased risk to certain cancers and diseases when there are abnormalities in the pathway.¹⁶⁻¹⁸ MUTYH-associated polyposis (MAP) is a form of inherited colorectal cancer where inheritance of functionally defective MUTYH variants leads to mutations in tumor suppressor genes.^{2, 15, 19, 20} Knowledge of defects in repair associated with specific cancers and tumor types has also led to increased interest in developing specific inhibitors for DNA repair enzymes.^{21, 22} This strategy is illustrated by the development of inhibitors of poly (ADP-ribose) polymerase (PARP), an enzyme that detects and initiates repair of single-strand breaks; PARP inhibitors have shown particular promise in patients harboring *BRCA1* and *BRCA2* mutations.²³ Inhibitors for BER pathway enzymes (such as PARP1, APE1 and Pol β) are especially effective in combination with other chemotherapeutic agents or ionizing radiation.²⁴⁻²⁷

Developing specific inhibitors for a particular DNA glycosylase is challenging given that these enzymes act upon subtle base modifications and often have overlapping substrate specificities.²⁸ Kinetic isotope effect (KIE) measurements performed on Uracil-DNA glycosylase (UDG) and MutY indicated these glycosylases catalyze *N*-glycosidic bond hydrolysis through a highly dissociative S_N1 mechanism featuring oxacarbenium ion

transition states (TS), TS1 and TS2 (Fig. 1B).^{29–31} Pyrrolidine nucleotides are a potent class of inhibitors for Ricin and DNA glycosylases, as the positive charge residing within the ring mimics the positive charge that accumulates in the oxacarbenium ion TSs and intermediates (Fig. 1C).^{32–36} Duplexes containing the TS analogs (Fig. 1C) exhibit exceptionally high affinity for BER glycosylases, and this high affinity has been exploited in structural studies to reveal interesting features of the mechanisms used by several glycosylases in damage recognition and base excision.^{37–40} For example, the X-ray structure of *Geobacillus stearothermophilus* (*Gs*) MutY bound to a duplex containing the TS mimic 1N opposite OG (referred to as transition state analog complex, TSAC) indicated approach of the water nucleophile from the same side as the departing base; this structural inference was confirmed by establishing that methanolysis catalyzed by *Gs* MutY proceeds with retention of stereochemistry.³⁷ Based on these insights obtained from TS mimics, a revised mechanism for MutY with similarities to that of “retaining” O-glycosidases was proposed involving two S_N1-like displacement steps and formation of a transient covalent DNA-enzyme intermediate (Fig S1).³⁷

An approach to specifically target a desired glycosylase would entail mimicry of TS1 by appending a base-like group to the pyrrolidine scaffold. TS1 mimics would provide a means to capitalize on differences in substrate specificity to target a glycosylase of interest. In addition, we anticipate that some glycosylases may utilize base recognition in the TS while others do not, and therefore the preferences for different TS1 mimics will reveal how recognition and excision are coupled by a particular BER glycosylase. In previous work, we showed that several glycosylases exhibit high affinity for oligonucleotides with TS1 mimics 1NBn, and TS2 analogs 4N and 1N (Fig. 1C);³⁶ notably, hOGG1 showed a slight preference for 1NBn over 4N and 1N, suggesting that elaboration of 1N with base-like moieties may provide TS1 mimics that retain high affinity but also exhibit higher specificity for one glycosylase over another. Identifying high affinity ligands to a given BER glycosylase would represent an important step toward developing specific glycosylase inhibitors.

TS1-specific transition state analogs are rare (Fig. 1C), and this may be due to the difficulty of synthesizing molecules that sufficiently resemble the natural substrates, but can also withstand the rigors of solid phase DNA synthesis. Copper (I)-catalyzed azide-alkyne cycloaddition (CuAAC), termed “click” chemistry, has often been used in applications with nucleic acids, including molecular diagnostics, fluorescent labeling, and DNA purification.⁴¹ Along with generally high yields and mild reaction conditions, CuAAC is an ideal method for synthesizing a number of analogs quickly and easily.⁴² Herein, we report the development of triazole TS1 mimics starting from the synthesis of a propargyl-containing pyrrolidine phosphoramidite monomer (**1**), its incorporation into oligonucleotides (1N-Prop, **2**), and post-synthetic modification by CuAAC using various azides (**3**) (Scheme 1). The relative affinities of the DNA glycosylases *E. coli* MutY (Ec MutY), Fpg, and hOGG1 for the elaborated TS1 mimics were determined using electrophoretic mobility shift assays. All three glycosylases exhibit exceptionally high affinity for the click-derived TS1 mimics. Notably, however, each glycosylase displays unique preferences within the TS1 mimic library indicating the power of this approach for identifying highly specific high-affinity ligands for BER glycosylases.

Results and Discussion

Synthesis of Clickable TS Mimic-Containing Oligonucleotides

The (3*R*, 4*R*)-(hydroxymethyl) pyrrolidin-3-ol (1N, **4**) nucleoside was synthesized in 14% overall yield in six steps using methods previously described.³⁶ Direct alkylation of 1N (**4**) with propargyl bromide resulted in over-alkylation at the secondary amine, and we therefore devised a reductive alkylation strategy to introduce the propargyl functional group, inspired by an analogous strategy applied by Tajbakhsh *et al.* for a series of secondary amines and aldehydes (Figure 2).⁴³ The alkyne functional group was incorporated using commercially available 3-(trimethylsilyl)-2-propynal due to its compatibility with automated solid-phase DNA synthesis. 1N was treated with 3-(trimethylsilyl)-2-propynal in the presence of sodium triacetoxyborohydride in ethanol for 2 hours to provide 1N with the appended TMS-propargyl handle (**5**) in 62% yield. The reaction was also found to proceed with sodium borohydride; however, the milder reducing agent sodium triacetoxyborohydride produced higher yields and prevented reduction of the alkyne to the alkene. Reactions were also found to proceed in similar yields in ethanol and 2,2,2-trifluoroethanol solvents. Protection of the 5'-hydroxyl with 4,4'-dimethoxytrityl chloride (DMTrCl) was completed in 51% yield, and phosphorylation of the 3'-hydroxyl with 2-cyanoethyl *N,N*-diisopropylchlorophosphoramidite produced the desired phosphoramidite, **1** (Figure 2A). Phosphoramidite **1** was incorporated into two DNA sequences containing 11 (**S11**) and 30 nucleotides (**S30**), respectively (Figure 2B). After deprotection and HPLC purification, the identity of each full-length oligonucleotide was verified by mass spectrometry (ESI-MS) (Table S1).

Synthesis of a Click TS1 mimic Library

Initial studies for TS mimic diversification by CuAAC used the alkyne-bearing 11-nucleotide sequence (**S11**, Figure 2B) and a set of five azides that varied in size, shape and polarity (Figure 2A). Specifically, this included the following azides: sodium azide (Az), azidobenzene (AzBen), 1-(2-azidoethyl)-1*H*-1,3-benzodiazole (AzBzD), 3-azidopropane-1-2-diol (AzDiol), and *N*-acetylglucosaminyl-*b*-propylazide (GlcNAc**ProN**₃).⁴⁴ Triazole products (1N-TriR) were generated by incubating an aqueous solution of **S11** (0.4 mM), tris-(hydroxypropyltriazolylmethyl)amine (THPTA, 10 mM), CuSO₄ (5 mM), sodium ascorbate (10 mM), and azide (4 mM) for 4–6 hours at room temperature in water or water/DMSO.⁴⁵ Reactions were quenched by dilution (80% formamide, 10 mM EDTA) and products were resolved from starting material using denaturing polyacrylamide gel electrophoresis (PAGE) (Fig. S2 & S3). With all five azides, reactions proceeded to completion with few side products as evident by observation of a single prominent band with slower mobility than that observed for the unreacted alkyne-containing oligonucleotide (e.g. Fig. S2, lane 1). The 1N-TriR containing oligonucleotide products were extracted from PAGE gels and their integrity was verified by mass spectrometry (ESI-MS) (Table S2). Similar methods were used to prepare the 1N-Prop containing 30-nucleotide sequence **S30**. Due to the longer length of **S30**, we were unable to observe differences in PAGE mobility for the product after the click reaction versus the starting oligonucleotide; however, after gel extraction, analysis by ESI-MS indicated complete conversion to the 1N-TriR products (Table S3).

These results establish an expedient method to prepare an appropriately protected propargyl containing 1N TS analog phosphoramidite monomer that can be incorporated into any desired DNA sequence using standard automated solid phase DNA synthesis and readily diversified using CuAAC click chemistry. As illustrated with a small library of five azides, the click reactions produced triazole products in near quantitative yield for both the 11 and 30-nucleotide sequences. Previous reports have shown that short alkynyl linkers in the context of oligonucleotides may be partially shielded by the DNA backbone, preventing access by azide;⁴⁶ however, this was not an issue with the alkyne-bearing TS mimic oligonucleotides. This may be due to placement of the alkyne-functionality at the position of the base allowing it to project away from the phosphodiester backbone into a DNA groove. An advantage of this approach is that it provides a means to prepare a diverse set of TS1 mimic oligonucleotides starting with a single oligonucleotide. Moreover, this method will allow for screening of a variety of TS1 mimics embedded within different DNA sequences, lengths and contexts. For the work presented here we analyzed the glycosylase affinity with DNA in duplex form, but the approach should work equally well with single-stranded, hairpin, and G-quadruplex DNA.

Stability of DNA containing click-derived TS mimics

Thermal denaturation (T_m) studies were conducted for the 1N-TriR TS1 mimic positioned opposite C in duplex DNA (D11) and relevant control duplexes to assess consequences of the substitutions on duplex stability (Table S4). The T_m measurements showed that duplexes containing the TS1- and TS2-mimic nucleotides are less stable than the natural G:C base pair (bp)-containing counterpart, with a range of relative destabilization (T_m ranging from -1.9 to -13.4 °C). Surprisingly, introduction of 1N-Prop and many of the 1N-TriR-containing nucleotides within the duplexes was generally less destabilizing relative to the TS2 analogs 1N and 4N. The 1N-Tri:C-containing duplex was the most stable DNA duplex tested with a T_m only 1.9 °C less than the corresponding G:C-containing duplex control. The stability of the 1N-Tri-containing DNA may be due to the heterocyclic triazole mimicking the nucleobase. Duplex stability was reduced with the larger 1N-TriBen and 1N-TriBzD-containing duplexes relative to 1N-Tri (Table 1). Curiously, 1N-TriDiol and 1N-TriGlcNAc-containing duplexes were not as destabilized as duplexes containing 1NBn, despite being larger modifications suggesting that the linker may provide flexibility to alleviate some of the steric duplex destabilization. These results illustrate that a diverse array of TS1 mimics prepared via click chemistry may be accommodated within DNA with only modest reductions in stability.

High affinity of TS1 Mimics for MutY and Impacts of Size

The affinity of *Escherichia coli* (Ec) MutY with the series of TS1 mimics was assessed using electrophoretic mobility shift assays (EMSA) to measure the relative K_d values.³⁶ Remarkably, MutY exhibits exceptionally high affinity for all the TS1 mimics in duplexes where the TS mimic is paired with OG (Figure S4). Using the lowest concentration of ³²P-labeled DNA that may be detected by storage phosphor autoradiography (5 pM duplex), we observed complete binding of duplex DNA even at the lowest MutY concentration used (10 pM). Based on the DNA concentration, we estimate an upper limit for the K_d value of 5 pM.

Ec MutY also exhibits adenine removal activity toward G:A mismatches^{2, 15} and we have previously shown that replacing OG with G in the duplex retains exceptionally high affinity for 1N ($K_d < 5$ pM), while significantly lowering affinity for the corresponding THF product analog duplex (2000 ± 1000 pM).³⁷ Similarly, using duplexes pairing 1N-Prop and 1N-TriR across from G revealed distinct selectivity of MutY imparted by the N1' substituent. The series of K_d values show that Ec MutY had higher affinity for 1N-TriR containing duplexes when R was smaller in size (Fig. 3 (red triangles), Table S5). For example, Ec MutY exhibited the highest affinity for DNA duplexes containing the smallest TS1 mimics, 1N-Prop and 1N-Tri, opposite G ($K_d \sim 100$ pM). The larger TS1 mimic 1NBn imparted slightly weaker affinity ($K_d \sim 500$ pM), and this trend continued for 1N-TriBen and 1N-TriDiol with measured K_d values of 600 and 700 pM, respectively. Ec MutY exhibited the weakest relative affinity for the two largest triazole-containing duplexes, 1N-TriBzD and 1N-TriGlcNAc, with the K_d values increasing into the nanomolar range. These results suggest that optimal positioning of the TS mimic within the MutY active site is influenced by the size of the appended base substituent, such that accommodation of larger groups incurs loss of optimal interactions. As described below, this size-dependent pattern is apparently unique to MutY; affinities measured for the other glycosylases (Fpg, hOGG1) did not strongly correlate with size (Fig. 3).

Differential Recognition of TS1 Mimics by Fpg and hOGG1

The relative affinities of OG glycosylases Fpg and hOGG1 were determined with the 30-bp duplex containing 1N-Prop and 1N-TriR derivatives positioned opposite C. We had previously observed that Fpg bound to DNA containing the TS analogs 4N, 1N, 1NBn and product analog THF with exceptionally high affinity (\sim pM) and did not discriminate between the positively charged TS analogs and the uncharged THF product analog.³⁶ Similarly, Fpg exhibited extremely high affinity for all of the duplexes containing 1N-Prop and 1N-TriR (Fig. 3 (green triangles) and S5). Based on the concentration of radiolabeled duplex used in the assay, we estimate the $K_d < 5$ pM for the entire series of TS1-mimic containing duplexes.

The binding curves for hOGG1 with duplexes containing 1N-Prop, -Tri, -TriBzD, -TriDiol, or -TriGlcNAc were best fit using a two-site binding isotherm that provided two distinct apparent K_d values (Fig. 3 (blue dots), Fig. 4, Table 2, Fig. S6). We have observed this type of binding behavior previously with hOGG1 and 1N, 4N, 1NBn and THF paired with C.³⁶ With the series of TS mimics, the apparent K_d values (Table 2) for the high-affinity site were too low (< 5 pM) to be accurately measured due to experimental limitations. A notable exception was observed with the 1N-TriGlcNAc-containing duplex where a reduced K_d of 16 pM at the high-affinity site was observed. For most of the duplexes tested, a second low affinity site of hOGG1 was observed with K_d values in the low nanomolar range (Table 2). Although hOGG1 binding with this series of TS mimic-containing duplexes generally exhibited comparable K_d values for the two sites, the *capacities* based on the fitting for K_d values were notably different. For example, DNA duplexes containing 1N-Prop, -TriBen, TriBzD, and -TriDiol showed a higher fraction ($> 75\%$) of complex forming with the low K_d value; we interpret this high affinity as binding within the substrate-binding site. The 1N-Tri and 1N-TriGlcNAc duplexes showed lower fractions of 59% and 39%, respectively, for this

high-affinity site (Table 2). Apparently, when the substituent appended to 1N more accurately mimics the substrate a higher population of the DNA is bound in the high-affinity substrate-binding site, while less faithful mimics are more likely to occupy the *exo* (also known as anti-substrate) site.

Notably, inspection of these results reveals that hOGG1 prefers TS1 mimics with base-like moieties over TS2 mimics, observable as a higher fraction of the TS1 duplexes binding in the high-affinity site. Indeed, the binding titration of hOGG1 with TS2 mimics 4N and 1N exhibited capacities of 50% and 36%, respectively, for the high-affinity site. 1N-Tri containing duplexes, interestingly, only displayed a slightly higher binding capacity for the high-affinity site (59%) than that of 4N and 1N, despite being the least sterically demanding mimic in the 1N-TriR series of analogs. Of particular note, hOGG1 exhibits almost complete binding (~92%) of the 1N-TriBen-containing duplex in the high-affinity site suggesting this TS1 mimic hits the “sweet spot” for hOGG1 (Figure 4). The trends for binding of the series of TS1 mimics with hOGG1 are distinctly different than binding trends for MutY and Fpg (Fig. 3). The Fpg glycosylase binds with high affinity to all of the TS1 mimics as does MutY when the TS1 mimic is paired with OG. In the case of MutY, replacement of OG with G reduced affinity sufficiently to reveal differences due to size of the elaborating group. In contrast, hOGG1 shows distinctly different binding behavior with two distinct sites, and a preference for the TS1 mimic 1N-TriBen.

Affinity of TS1 mimics implicates an Adenine exit channel of MutY

The impact of the appended substituent of the TS1 mimics paired with G on the measured K_d values of Ec MutY suggests that interactions with the nucleobase are important in stabilizing TS1. In the co-crystal structure of Gs MutY bound to noncleavable 2'-fluoroadenosine substrate analog (PDB ID: 3G0Q; referred to as the *fluorinated lesion-recognition complex* or FLRC, Fig. S7a), extensive contacts are made to the adenine nucleobase.⁴⁷ In particular, hydrogen bonds are formed between Glu43, Tyr126, and N7 of adenine. Arg31 and Trp30 are also within hydrogen-bonding distances to N1 and the N6 exocyclic amine of adenine.⁴⁷ When compared to the TSAC structure of a duplex containing a central OG:1N bp bound by Gs MutY (PDB ID: 5DPK) (Fig. S7b,c), the interaction between Tyr126 and Glu43 with N7 of adenine was replaced with a hydrogen bond network to the positively charged and protonated nitrogen in 1N.³⁷ This network included a water molecule that is strongly suspected to be the water nucleophile because of its close distances to 1N and the catalytic residue Glu43, and because its position on the 5' face of 1N is consistent with retaining stereochemistry determined for methanolysis catalyzed by MutY.³⁷ Adenine was not observed in the TSAC structure, and the suspected water nucleophile occupies the position of adenine in the FLRC.³⁷ These structural rearrangements inferred from comparison of FLRC and TSAC structures suggest that catalysis is accompanied by tighter interactions with the oxacarbenium ion intermediate (and TS2) that effectively move the adenine base out of the active site, making the enzyme-catalyzed reaction essentially irreversible.³⁷

The 1N-Tri, -TriDiol, and -TriBzD TS1 analogs were modeled into the TSAC structure with the goal of rationalizing differences in affinity of MutY for the series of TS1 mimics.

Analysis of the TSAC structure indicates two access portals from the surface of the enzyme to the active site, one of which is large enough for access of water, and the other that may be large enough to serve as the adenine exit tunnel (Fig. 5). Indeed, there was significant space along the suspected adenine exit tunnel to accommodate the 1N-Tri analog (Fig. 5, Table S6). In creating this model, a number of steric clashes between MutY and 1N-Tri were avoided by adjustments to torsion angles in the 5-membered ring of 1N, suggesting significantly different sugar puckers in TS1 (modeled by 1N-Tri) and TS2 (mimicked by 1N). The propane diol substituent of 1N-TriDiol is extended further into the adenine exit tunnel without major steric conflicts (Fig. S8, Table S6). Although 1N-TriBzD has shape complementarity to adenine, the modeled structure showed several clashes between the TriBzD side chain and residues in the adenine exit portal (Fig. 5, Table S6). Presumably, residues lining the exit channel adopt alternate, less stable conformations to avoid these predicted clashes, and this may be the source of reduced affinity for this analog (Fig. 3, Table S5).

Given the observed trend of MutY-DNA affinity and the clashes predicted for TriBzD, it was somewhat surprising that 1N-TriGlcNAc, binds only slightly less tightly than does 1N-TriBzD. The TriGlcNAc group is expected to completely penetrate through the proposed adenine exit tunnel, with several additional clashes along the way. The rather small impact of additional predicted clashes may be explained by two, not necessarily exclusive, molecular mechanisms. In one mechanism, a concerted rearrangement of residues lining the exit channel, triggered by mild steric clashes leads to a more accommodating larger tunnel. Alternatively, the larger groups attached to 1N may prevent this part of the DNA structure from entering the active site. Indeed, structure determination for OG:C anti-substrate DNA in complex with MutY revealed an *exo* site distinct from the active site, demonstrating that a continuous DNA backbone can avoid the active site.⁴⁸ It will be interesting to see which model is correct through structure determination for MutY in complex with Tri-substituted DNA. Overall, the structural models show that TS1 mimics can be accommodated in an extended active site and suggest a plausible route for adenine exit through a tunnel to bulk solvent.

High affinity of Fpg with large 1N-TriR TS1 Mimics

It is rather remarkable that Fpg was able to accommodate the larger 1N-TriBzD and 1N-TriGlcNAc TS mimics with such high affinity. Crystal structures of catalytically inactive *Geobacillus stearothermophilus* Fpg (E3Q) bound to an OG:C containing DNA showed extensive protein contacts to the OG nucleobase in the *syn* conformation.⁵⁰ Interestingly, the lesion-recognition loop making these OG contacts is not observed in crystal structures devoid of a lesion nucleobase, suggesting that this loop is naturally disordered and flexible in non-lesion contexts. Further evidence for conformational flexibility may be gleaned from inspection of the X-ray crystal structure of catalytically inactive *Lactococcus lactis* Fpg (P1-L/Fpg) that showed the lesion-recognition loop nestled around the carbocyclic FapyG lesion, but with the base in the *anti* conformation.⁵¹ These structures illustrate the nimbleness of Fpg to accommodate base lesions with varying structures and in different orientations relative to the DNA backbone, consistent with the broad substrate scope of this glycosylase.

In order to rationalize the observed high affinity of Fpg for the 1N-TriR series with no apparent dependence on the size of the appended R group, a structural model was generated on the basis of R247G *L*Fpg bound to lesion-containing DNA (PDB ID: 4PCZ). In the resulting model, Fpg binds the 1N-TriR DNA duplex by projecting the R substituent into a solvent exposed pocket (Fig. 6).⁵² Similar models generated with a viral ortholog of hNEIL1 helped rationalize its high activity toward removal of Sp-amine adducts containing a large appended peptide.⁵³ Structural studies of the AlkD glycosylase provide insight into an alternative strategy used by glycosylases to remove bulky lesions by tucking the large adduct into the DNA minor groove rather than completely extruding the base from the helix.³⁸ These studies along with the results herein further dispel dogma that BER glycosylases bind their substrate base within a snug base-binding pocket. Moreover, these models suggest that Fpg may bind with high affinity to 1N-TriR TS mimics that are even larger than 1N-TriBzD or 1N-TriGlcNAc, and this feature may provide a unique strategy to selectively target a desired DNA repair glycosylase. Indeed, use of a TS1 mimic containing a large appendage would be expected to retain high affinity for Fpg, but not for MutY, providing the means to specifically inhibit Fpg.

1N-TriR TS1 mimics are accommodated within two distinct sites in hOGG1

The two distinct K_d values observed with hOGG1 suggest that the DNA duplex can bind in two distinct orientations or sites within hOGG1. Consistent with this idea, structural studies of BER enzymes have shown the binding of potential substrates and anti-substrates at distinct sites.^{54–56} In hOGG1, these two sites are thought to be used as a mechanism to faithfully recognize and excise OG over G by intercepting G bases in an *exo* site and preventing its full-engagement in the active site. The high occupancy of the high-affinity site suggests that the Tri-Ben substituent is accommodated by hOGG1 in a way that allows for complete engagement in the active site. Indeed, modeling of 1N-TriBen into DNA duplex co-crystal structures of hOGG1 and OG (PDB ID: 1YQR) and G (PDB ID:1YQK) showed that the TriBen substituent could be accommodated in both the active- and *exo*-site pockets (Fig. 7).⁵⁵ These results suggest an exciting possibility for further development of site-specific and high-affinity inhibitors for hOGG1. Site-specific inhibitors of hOGG1 coupled with structural studies may shed light on the subtlety and complexity of precise recognition and excision of OG by hOGG1. Moreover, high-affinity and site-specific inhibitors of hOGG1 would be useful chemical biology tools to decipher the impact of inhibition of hOGG1 in cells.

Concluding Remarks

Targeting glycosylases involved in oxidative base repair is particularly attractive since the high levels of oxidative stress in cancer cells would be expected to provide sensitivity to inhibition of these repair pathways.^{21, 22} In addition, DNA repair defects that serve as initiating events in carcinogenesis are often the Achilles heel of cancer cells due to the increased reliance on the remaining intact DNA repair pathways.²⁷ Indeed, hOGG1 has emerged as a promising chemotherapeutic target and there have been two recent reports of small molecule inhibitors for hOGG1.^{57, 58} In these reports, screening of small molecule libraries was used as a means to identify specific inhibitors for hOGG1. In contrast, we have

developed a new approach where a library of tight-binding TS mimic oligonucleotides are prepared using a post-synthetic CuAAC reaction to allow for screening for glycosylase specific binding. This is the first example of this reaction utilized in the context of a transition state mimic-containing DNA or RNA oligonucleotide. This method will allow for development of tight-binding inhibitors relatively quickly compared to traditional methods. We have shown that these 1N-based TS mimics bind with extremely high affinity to DNA glycosylases Ec MutY, hOGG1, and Fpg. Moreover, using the small set of analogs prepared herein we identified a distinct preference of hOGG1 for a particular TS1 mimic (1N-TriBen), a preference of MutY for small TS1 mimics, and a tolerance by Fpg for very large TS1 mimics. In addition, the differences in affinity of the three glycosylases due to the size and shape of the TS1 mimics, coupled with modeling using co-crystal structures, has provided interesting insight into features of the recognition and excision process used by these three similar, but distinct, glycosylases. These enzyme-specific trends provide evidence that this click-based strategy for preparation of TS mimics combined with high-throughput biochemical assays will be particularly powerful in the development of highly specific and tight-binding BER glycosylase inhibitors.

Supplementary Material

Refer to Web version on PubMed Central for supplementary material.

ACKNOWLEDGEMENTS

This work was supported by the National Science Foundation (CHE-1610721 to S.S.D. and CHE-1608934 to M.P.H.) and NIH grant R01A1130684 to X.C. K.T.L. was supported by the UCD NIH Chemical Biology Training Program (T32-GM113770). J.A. was a trainee on the T32 training grant in Oncogenic Signals and Chromosome Biology (T32-CA10859) and a Ford Foundation Fellowship.

REFERENCES

- [1]. Lindahl T (1993) Instability and decay of the primary structure of DNA, *Nature* 362, 709–715. [PubMed: 8469282]
- [2]. David SS, O’Shea VL, and Kundu S (2007) Base-excision repair of oxidative DNA damage, *Nature* 447, 941–950. [PubMed: 17581577]
- [3]. Krokan HE, and Bjoras M (2013) Base excision repair, *Cold Spring Harb Perspect Biol* 5, a012583. [PubMed: 23545420]
- [4]. Wilson DL, (Ed.) (2017) *The Base Excision Repair Pathway: Molecular Mechanisms and Roles in Disease Development and Therapeutic Design*, World Scientific Publishing Co, New Jersey.
- [5]. David SS, and Williams SD (1998) Chemistry of Glycosylase and Endonuclease involved in Base-Excision Repair, *Chem. Rev* 98, 1221–1261. [PubMed: 11848931]
- [6]. Robertson AB, Klungland A, Rognes T, and Leiros I (2009) DNA repair in mammalian cells: Base excision repair: the long and short of it, *Cell Mol Life Sci* 66, 981–993. [PubMed: 19153658]
- [7]. Prakash A, Doublie S, and Wallace SS (2012) The Fpg/Nei family of DNA glycosylases: substrates, structures, and search for damage, *Prog Mol Biol Transl Sci* 110, 71–91. [PubMed: 22749143]
- [8]. Dalhus B, Laerdahl JK, Backe PH, and Bjoras M (2009) DNA base repair--recognition and initiation of catalysis, *FEMS Microbiol Rev* 33, 1044–1078. [PubMed: 19659577]
- [9]. Greenberg MM (2012) The formamidopyrimidines: purine lesions formed in competition with 8-oxopurines from oxidative stress, *Acc Chem Res* 45, 588–597. [PubMed: 22077696]
- [10]. Jacobs AL, and Schar P (2012) DNA glycosylases: in DNA repair and beyond, *Chromosoma* 121, 1–20. [PubMed: 22048164]

- [11]. Saparbaev M, Sidorkina OM, Jurado J, Privezentzev CV, Greenberg MM, and Laval J (2002) Repair of oxidized purines and damaged pyrimidines by *E. coli* Fpg protein: different roles of proline 2 and lysine 57 residues, *Environ Mol Mutagen* 39, 10–17. [PubMed: 11813291]
- [12]. Krishnamurthy N, Muller JG, Burrows CJ, and David SS (2007) Unusual structural features of hydantoin lesions translate into efficient recognition by *Escherichia coli* Fpg, *Biochemistry* 46, 9355–9365. [PubMed: 17655276]
- [13]. Leipold MD, Muller JG, Burrows CJ, and David SS (2000) Removal of hydantoin products of 8-oxoguanine oxidation by the *Escherichia coli* DNA repair enzyme, FPG, *Biochemistry* 39, 14984–14992. [PubMed: 11101315]
- [14]. McKibbin PL, Kobori A, Taniguchi Y, Kool ET, and David SS (2012) Surprising repair activities of nonpolar analogs of 8-oxoG expose features of recognition and catalysis by base excision repair glycosylases, *J Am Chem Soc* 134, 1653–1661. [PubMed: 22175854]
- [15]. Banda DM, Nunez NN, Burnside MA, Bradshaw KM, and David SS (2017) Repair of 8-oxoG:A mismatches by the MUTYH glycosylase: Mechanism, metals and medicine, *Free radical biology & medicine* 107, 202–215. [PubMed: 28087410]
- [16]. Friedberg EC (2003) DNA damage and repair, *Nature* 421, 436–440. [PubMed: 12540918]
- [17]. Wallace SS, Murphy DL, and Sweasy JB (2012) Base excision repair and cancer, *Cancer Lett* 327, 73–89. [PubMed: 22252118]
- [18]. Scott TL, Rangaswamy S, Wicker CA, and Izumi T (2014) Repair of oxidative DNA damage and cancer: recent progress in DNA base excision repair, *Antioxid Redox Signal* 20, 708–726. [PubMed: 23901781]
- [19]. Nielsen M, Morreau H, Vasen HF, and Hes FJ (2011) MUTYH-associated polyposis (MAP), *Crit Rev Oncol Hematol* 79, 1–16. [PubMed: 20663686]
- [20]. Lipton L, Halford SE, Johnson V, Novelli MR, Jones A, Cummings C, Barclay E, Sieber O, Sadat A, Bisgaard ML, Hodgson SV, Aaltonen LA, Thomas HJ, and Tomlinson IP (2003) Carcinogenesis in MYH-associated polyposis follows a distinct genetic pathway, *Cancer Res* 63, 7595–7599. [PubMed: 14633673]
- [21]. Helleday T, Petermann E, Lundin C, Hodgson B, and Sharma RA (2008) DNA repair pathways as targets for cancer therapy, *Nat Rev Cancer* 8, 193–204. [PubMed: 18256616]
- [22]. Lord CJ, and Ashworth A (2012) The DNA damage response and cancer therapy, *Nature* 481, 287–294. [PubMed: 22258607]
- [23]. Fong PC, Boss DS, Yap TA, Tutt A, Wu P, Mergui-Roelvink M, Mortimer P, Swaisland H, Lau A, O'Connor MJ, Ashworth A, Carmichael J, Kaye SB, Schellens JH, and de Bono JS (2009) Inhibition of poly(ADP-ribose) polymerase in tumors from BRCA mutation carriers, *N Engl J Med* 361, 123–134. [PubMed: 19553641]
- [24]. Bapat A, Fishel ML, and Kelley MR (2009) Going ape as an approach to cancer therapeutics, *Antioxid Redox Signal* 11, 651–668. [PubMed: 18715143]
- [25]. Shall S, Gaymes T, Farzaneh F, Curtin NJ, and Mufti GJ (2017) The Use of PARP Inhibitors in Cancer Therapy: Use as Adjuvant with Chemotherapy or Radiotherapy, Use as a Single Agent in Susceptible Patients, and Techniques Used to Identify Susceptible Patients, *Methods in molecular biology* (Clifton, N.J.) 1608, 343–370.
- [26]. Jaiswal AS, Banerjee S, Panda H, Bulkin CD, Izumi T, Sarkar FH, Ostrov DA, and Narayan S (2009) A novel inhibitor of DNA polymerase beta enhances the ability of temozolomide to impair the growth of colon cancer cells, *Molecular cancer research: MCR* 7, 1973–1983. [PubMed: 19996303]
- [27]. Curtin NJ (2012) DNA repair dysregulation from cancer driver to therapeutic target, *Nat Rev Cancer* 12, 801–817. [PubMed: 23175119]
- [28]. Schärer OD, Deng L, and Verdine GL (1997) Chemical approaches toward understanding base excision DNA repair, *Curr Opin Chem Biol* 1, 526–531. [PubMed: 9667887]
- [29]. Berti PJ, and McCann JA (2006) Toward a detailed understanding of base excision repair enzymes: transition state and mechanistic analyses of N-glycoside hydrolysis and N-glycoside transfer, *Chem Rev* 106, 506–555. [PubMed: 16464017]
- [30]. McCann JA, and Berti PJ (2008) Transition-state analysis of the DNA repair enzyme MutY, *J Am Chem Soc* 130, 5789–5797. [PubMed: 18393424]

- [31]. Werner RM, and Stivers JT (2000) Kinetic isotope effect studies of the reaction catalyzed by uracil DNA glycosylase: evidence for an oxocarbenium ion-uracil anion intermediate, *Biochemistry* 39, 14054–14064. [PubMed: 11087352]
- [32]. Hernández D, and Boto A (2014) Nucleoside analogues: synthesis and biological properties of azanucleoside derivatives, *European Journal of Organic Chemistry* 2014, 2201–2220.
- [33]. Schärer OD, Nash HM, Jiricny J, Laval J, and Verdine GL (1998) Specific binding of a designed pyrrolidine abasic site analog to multiple DNA glycosylases, *J Biol Chem* 273, 8592–8597. [PubMed: 9535832]
- [34]. Deng L, Schärer OD, and Verdine GL (1997) Unusually strong binding of a designed transition-state analog to a base-excision DNA repair protein, *J Am Chem Soc* 119, 7865–7866.
- [35]. Roday S, Amukele T, Evans GB, Tyler PC, Furneaux RH, and Schramm VL (2004) Inhibition of ricin A-chain with pyrrolidine mimics of the oxocarbenium ion transition state, *Biochemistry* 43, 4923–4933. [PubMed: 15109250]
- [36]. Chu AM, Fettingner JC, and David SS (2011) Profiling base excision repair glycosylases with synthesized transition state analogs, *Bioorg Med Chem Lett* 21, 4969–4972. [PubMed: 21689934]
- [37]. Woods RD, O'Shea VL, Chu A, Cao S, Richards JL, Horvath MP, and David SS (2016) Structure and stereochemistry of the base excision repair glycosylase MutY reveal a mechanism similar to retaining glycosidases, *Nucleic Acids Res* 44, 801–810. [PubMed: 26673696]
- [38]. Mullins EA, Shi R, Parsons ZD, Yuen PK, David SS, Igarashi Y, and Eichman BF (2015) The DNA glycosylase AlkD uses a non-base-flipping mechanism to excise bulky lesions, *Nature* 527, 254–258. [PubMed: 26524531]
- [39]. Hollis T, Ichikawa Y, and Ellenberger T (2000) DNA bending and a flip-out mechanism for base excision by the helix-hairpin-helix DNA glycosylase, *Escherichia coli* AlkA, *EMBO J* 19, 758–766. [PubMed: 10675345]
- [40]. Bianchet MA, Seiple LA, Jiang YL, Ichikawa Y, Amzel LM, and Stivers JT (2003) Electrostatic guidance of glycosyl cation migration along the reaction coordinate of uracil DNA glycosylase, *Biochemistry* 42, 12455–12460. [PubMed: 14580190]
- [41]. Gramlich PM, Wirges CT, Manetto A, and Carell T (2008) Postsynthetic DNA modification through the copper-catalyzed azide-alkyne cycloaddition reaction, *Angew Chem Int Ed Engl* 47, 8350–8358. [PubMed: 18814157]
- [42]. Hein JE, and Fokin VV (2010) Copper-catalyzed azide-alkyne cycloaddition (CuAAC) and beyond: new reactivity of copper(I) acetylides, *Chem Soc Rev* 39, 1302–1315. [PubMed: 20309487]
- [43]. Tajbakhsh M, Hosseinzadeh R, Alinezhad H, Ghahari S, Heydari A, and Khaksar S (2011) Catalyst-Free One-Pot Reductive Alkylation of Primary and Secondary Amines and N,N-Dimethylation of Amino Acids Using Sodium Borohydride in 2,2,2-Trifluoroethanol, *Synthesis* 2011, 490–496.
- [44]. Lau K, Thon V, Yu H, Ding L, Chen Y, Muthana MM, Wong D, Huang R, and Chen X (2010) Highly efficient chemoenzymatic synthesis of beta1–4-linked galactosides with promiscuous bacterial beta1–4-galactosyltransferases, *Chemical communications (Cambridge, England)* 46, 6066–6068.
- [45]. Peacock H, Maydanovych O, and Beal PA (2010) N(2)-Modified 2-aminopurine ribonucleosides as minor-groove-modulating adenosine replacements in duplex RNA, *Org Lett* 12, 1044–1047. [PubMed: 20108910]
- [46]. Gierlich J, Burley GA, Gramlich PM, Hammond DM, and Carell T (2006) Click chemistry as a reliable method for the high-density postsynthetic functionalization of alkyne-modified DNA, *Org Lett* 8, 3639–3642. [PubMed: 16898780]
- [47]. Lee S, and Verdine GL (2009) Atomic substitution reveals the structural basis for substrate adenine recognition and removal by adenine DNA glycosylase, *Proc Natl Acad Sci U S A* 106, 18497–18502. [PubMed: 19841264]
- [48]. Wang L, Lee SJ, and Verdine GL (2015) Structural Basis for Avoidance of Promutagenic DNA Repair by MutY Adenine DNA Glycosylase, *J Biol Chem* 290, 17096–17105. [PubMed: 25995449]

- [49]. Pettersen EF, Goddard TD, Huang CC, Couch GS, Greenblatt DM, Meng EC, and Ferrin TE (2004) UCSF Chimera--a visualization system for exploratory research and analysis, *J Comput Chem* 25, 1605–1612. [PubMed: 15264254]
- [50]. Fromme JC, and Verdine GL (2003) DNA lesion recognition by the bacterial repair enzyme MutM, *J Biol Chem* 278, 51543–51548. [PubMed: 14525999]
- [51]. Coste F, Ober M, Carell T, Boiteux S, Zelwer C, and Castaing B (2004) Structural basis for the recognition of the FapydG lesion (2,6-diamino-4-hydroxy-5-formamidopyrimidine) by formamidopyrimidine-DNA glycosylase, *J Biol Chem* 279, 44074–44083. [PubMed: 15249553]
- [52]. Biela A, Coste F, Culard F, Guerin M, Goffinont S, Gasteiger K, Ciesla J, Winczura A, Kazimierczuk Z, Gasparutto D, Carell T, Tudek B, and Castaing B (2014) Zinc finger oxidation of Fpg/Nei DNA glycosylases by 2-thioxanthine: biochemical and X-ray structural characterization, *Nucleic Acids Res* 42, 10748–10761. [PubMed: 25143530]
- [53]. McKibbin PL, Fleming AM, Towheed MA, Van Houten B, Burrows CJ, and David SS (2013) Repair of hydantoin lesions and their amine adducts in DNA by base and nucleotide excision repair, *J Am Chem Soc* 135, 13851–13861. [PubMed: 23930966]
- [54]. Crenshaw CM, Nam K, Oo K, Kutchukian PS, Bowman BR, Karplus M, and Verdine GL (2012) Enforced presentation of an extrahelical guanine to the lesion recognition pocket of human 8-oxoguanine glycosylase, hOGG1, *J Biol Chem* 287, 24916–24928. [PubMed: 22511791]
- [55]. Banerjee A, Yang W, Karplus M, and Verdine GL (2005) Structure of a repair enzyme interrogating undamaged DNA elucidates recognition of damaged DNA, *Nature* 434, 612–618. [PubMed: 15800616]
- [56]. van der Kemp PA, Charbonnier JB, Audebert M, and Boiteux S (2004) Catalytic and DNA-binding properties of the human Ogg1 DNA N-glycosylase/AP lyase: biochemical exploration of H270, Q315 and F319, three amino acids of the 8-oxoguanine-binding pocket, *Nucleic Acids Res* 32, 570–578. [PubMed: 14752045]
- [57]. Donley N, Jaruga P, Coskun E, Dizdaroglu M, McCullough AK, and Lloyd RS (2015) Small Molecule Inhibitors of 8-Oxoguanine DNA Glycosylase-1 (OGG1), *ACS chemical biology* 10, 2334–2343. [PubMed: 26218629]
- [58]. Tahara YK, Auld D, Ji D, Beharry AA, Kietrys AM, Wilson DL, Jimenez M, King D, Nguyen Z, and Kool ET (2018) Potent and Selective Inhibitors of 8-Oxoguanine DNA Glycosylase, *J Am Chem Soc* 140, 2105–2114. [PubMed: 29376367]

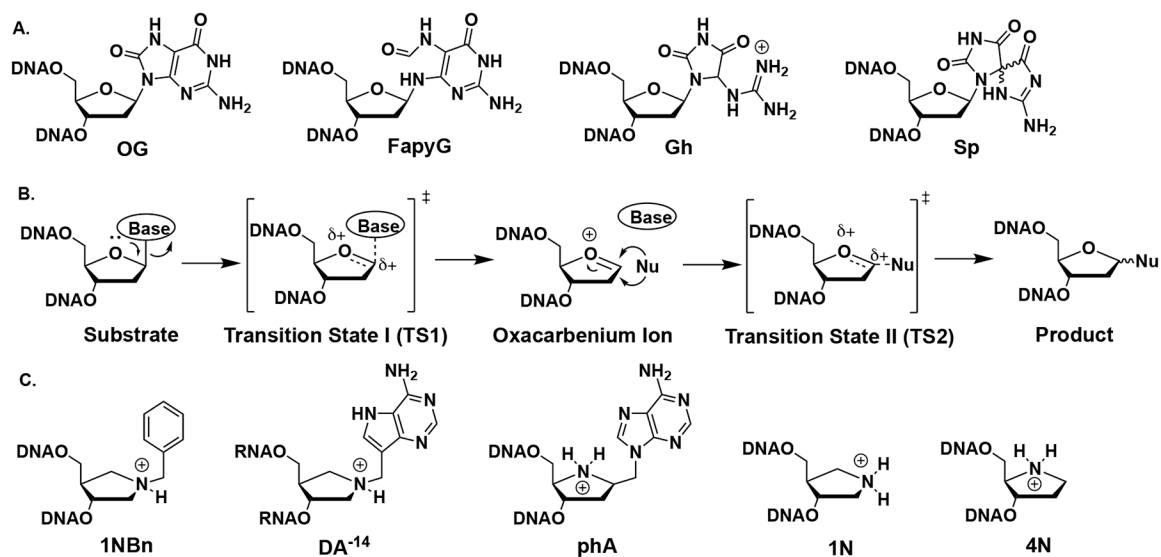
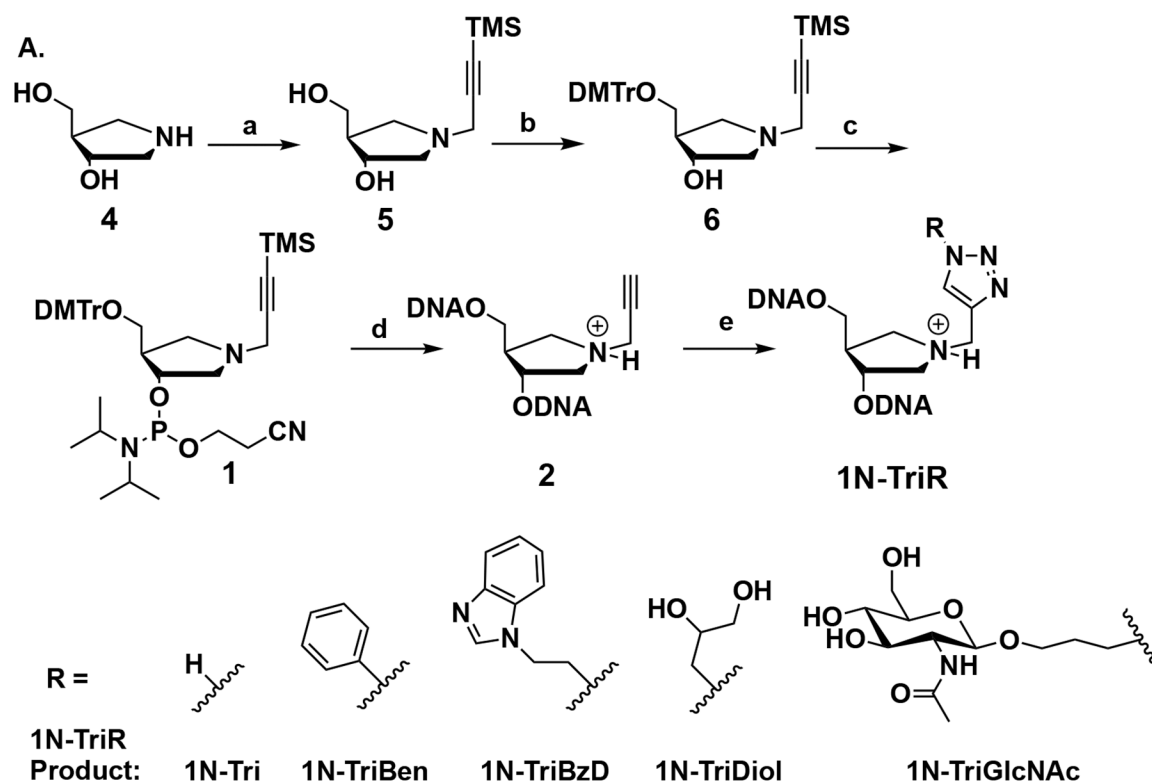


Figure 1: BER glycosylase substrates and mechanism.

(A) Examples of damaged bases removed by BER glycosylases. (B) The generally accepted S_N1 type mechanism for catalysis of N-glycosidic bond hydrolysis based on KIE studies by BER glycosylases. In the first step, the N-glycosidic bond breaks, giving rise to a highly reactive oxocarbenium ion intermediate, which is followed by nucleophilic attack on the anomeric carbon, providing the product. At least two transition states (TS)s, TS1 and TS2, can be envisioned during this process. (C) Structures of azasugar transition state analogs 1NBn, DA⁻¹⁴, phA, 1N, and 4N. DNA glycosylases exhibit extremely high binding affinity for duplexes containing azanucleotide TS analogs (< 5 pM).

**B.****S11: 5' - TGT CCA 2GT CT - 3'****S30: 5' - TGT TCA TGG GTC 2TC GGT ATA TCC CAT - 3'****Figure 2: Synthesis of TS mimic-containing oligonucleotides.**

(A) Synthesis of 1N-propargyl phosphoramidite, incorporation into DNA and diversification using Cu-catalyzed azide-alkyne cycloaddition. Synthetic conditions: a. 3-(Trimethylsilyl)-2-propyne, NaBH(OAc)₃, ethanol, room temperature, 2 hr, 62%; b. 4,4'-dimethoxytrityl chloride, pyridine, room temperature, 2 hr, 51%; c. *N,N*-diisopropylethylamine, 2-cyanoethyl-*N,N*-diisopropylchlorophosphoramidite, CH₂Cl₂, room temperature, 1.5 hr, 63%; d. Automated solid-phase DNA synthesis using UltraMild phosphoramidites and conditions. e. R-N₃, THPTA, CuSO₄, H₂O or H₂O/DMSO, 4–6 hrs.

(B) Sequence of oligonucleotides containing TS mimic. Duplexes used were prepared by annealing with the appropriate complementary sequence to position C, G or OG opposite the TS mimic (see methods for full duplex sequences).

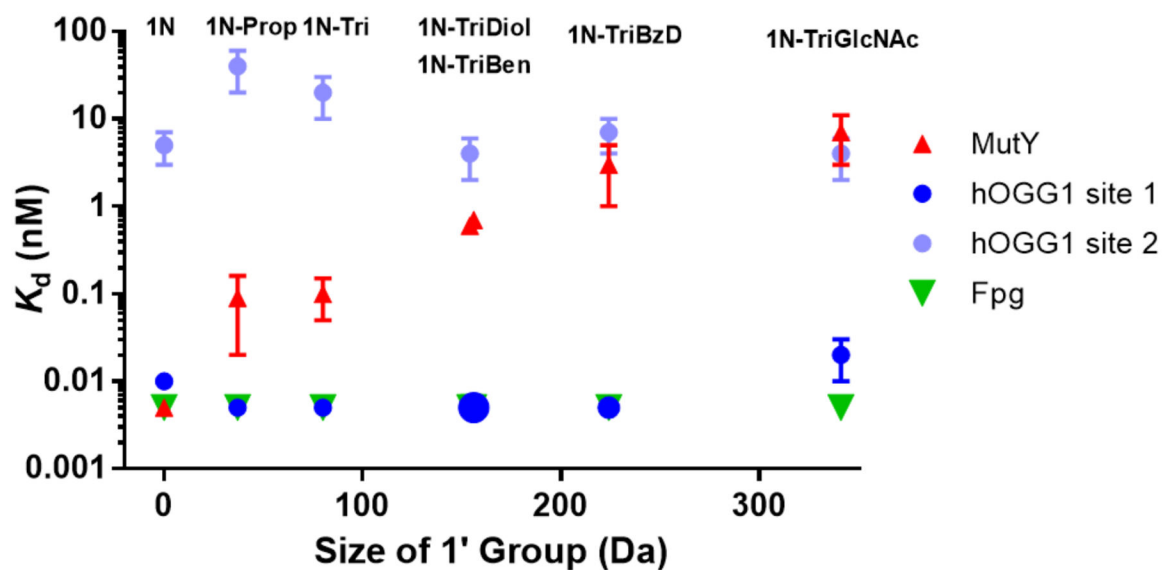


Figure 3: Binding Preferences of Fpg, hOGG1 and MutY with 1N-TriR duplexes.

Duplex DNA positions the TS mimic in the S30 sequence opposite C (hOGG1, Fpg) or G (MutY). Note, the TS2 mimic 1N has no substituent and is therefore plotted with a size of “0”. The K_d values for Fpg are an upper limit estimate ($K_d < 5$ pM). This is also the case for some MutY and hOGG1 K_d values. Refer to Table 2 and S5 for actual values. In the case of hOGG1, the relative capacities of the two K_d values are indicated by the size of the blue dot, for example, the large dot for 1N-TriBen reflects almost exclusive binding at the high affinity site (92%). Note that for the large substituents, such as 1N-TriGlcNAc, Fpg exhibits >1,400-fold higher affinity compared to that of MutY. Error bars show 95% confidence intervals.

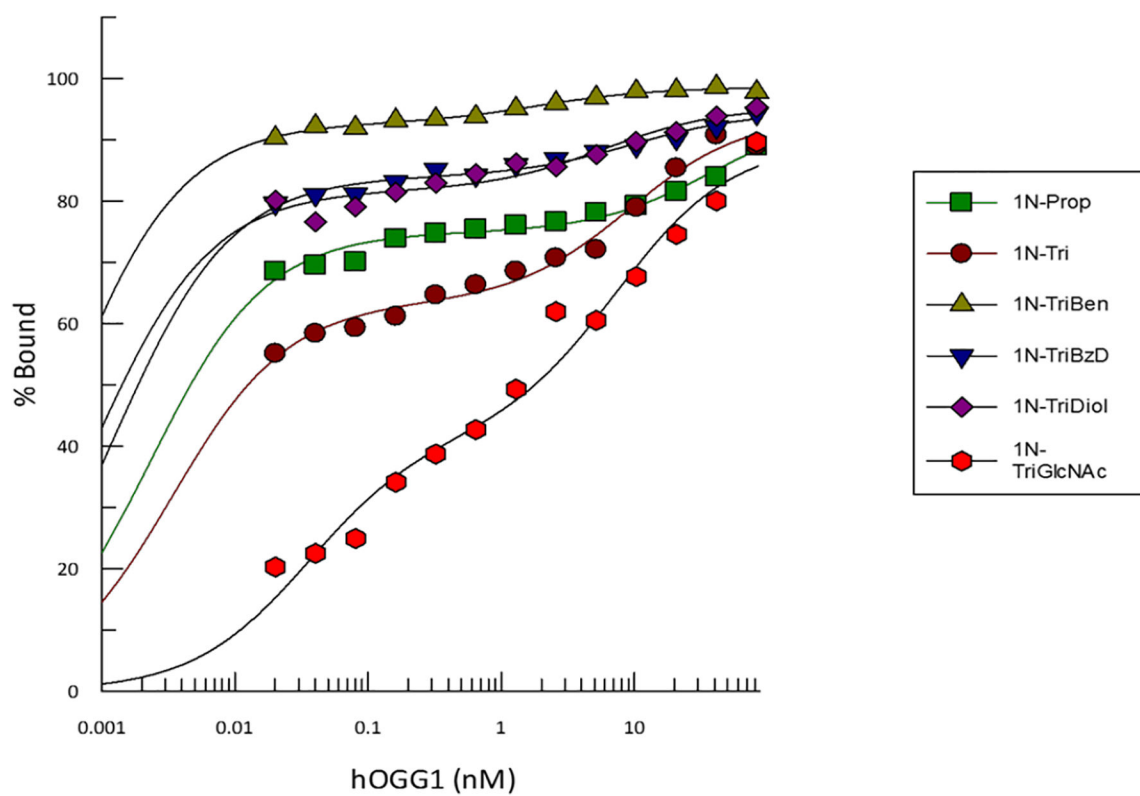


Figure 4: Affinity of hOGG1 for TS1 Mimics.

Shown is a representative plot of percent hOGG1 bound to 1N-Prop and 1N-TriR positioned opposite C in the 30 bp duplex. The data fit best using a two-site binding isotherm. Resulting K_d values are listed in Table 2.

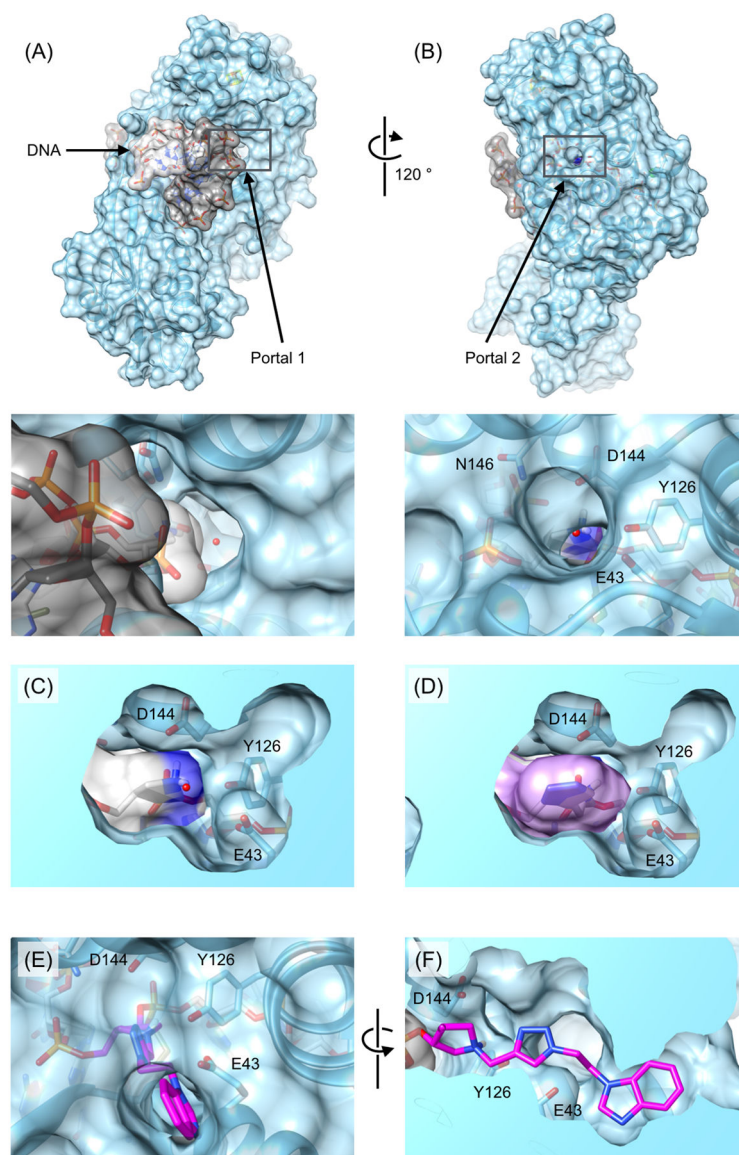


Figure 5: Structural models of DNA with 1N-TriR bound to MutY.

(A, B) Two portals are present in the TSAC structure of MutY: (A) Portal 1 is small and could provide water access to the 5' face of TS2; (B) Portal 2 is larger and provides a potential adenine exit route. The views shown in panels A and B are related by approximately 120° rotation. A close up of each portal is shown below the overview, with the suspect water nucleophile present as a red sphere. The two DNA strands are colored light and dark gray. The positively charged N1' amine of 1N is colored blue. Catalytic residues are labeled with single-letter abbreviations: N, Asn; D, Asp; E, Glu; Y, Tyr. (C) Cut-away view of 1N bound in the active site. (D) Cut-away view of 1N-Tri (violet) modeled into the active site of MutY. Note that the sugar pucker for 1N-Tri was adjusted relative to the 1'-exo pucker observed for 1N by x-ray structure determination so as to reduce steric clashes. (E, F) A model of 1N-TriBzD (magenta) positioned in the adenine exit tunnel is shown, looking into the adenine exit tunnel (E) and as a cutaway view of the exit tunnel (F). There are at

least 9 steric conflicts between the 1N-TriBzD group and residues belonging to MutY, far more than experienced for smaller 1N-TriR groups (Table S5). Figures and structural models prepared with UCSF chimera,⁴⁹ on the basis of the TSAC structure for OG:1N DNA bound to *Gs*MutY (PDB ID 5DPK).³⁷

Author Manuscript

Author Manuscript

Author Manuscript

Author Manuscript

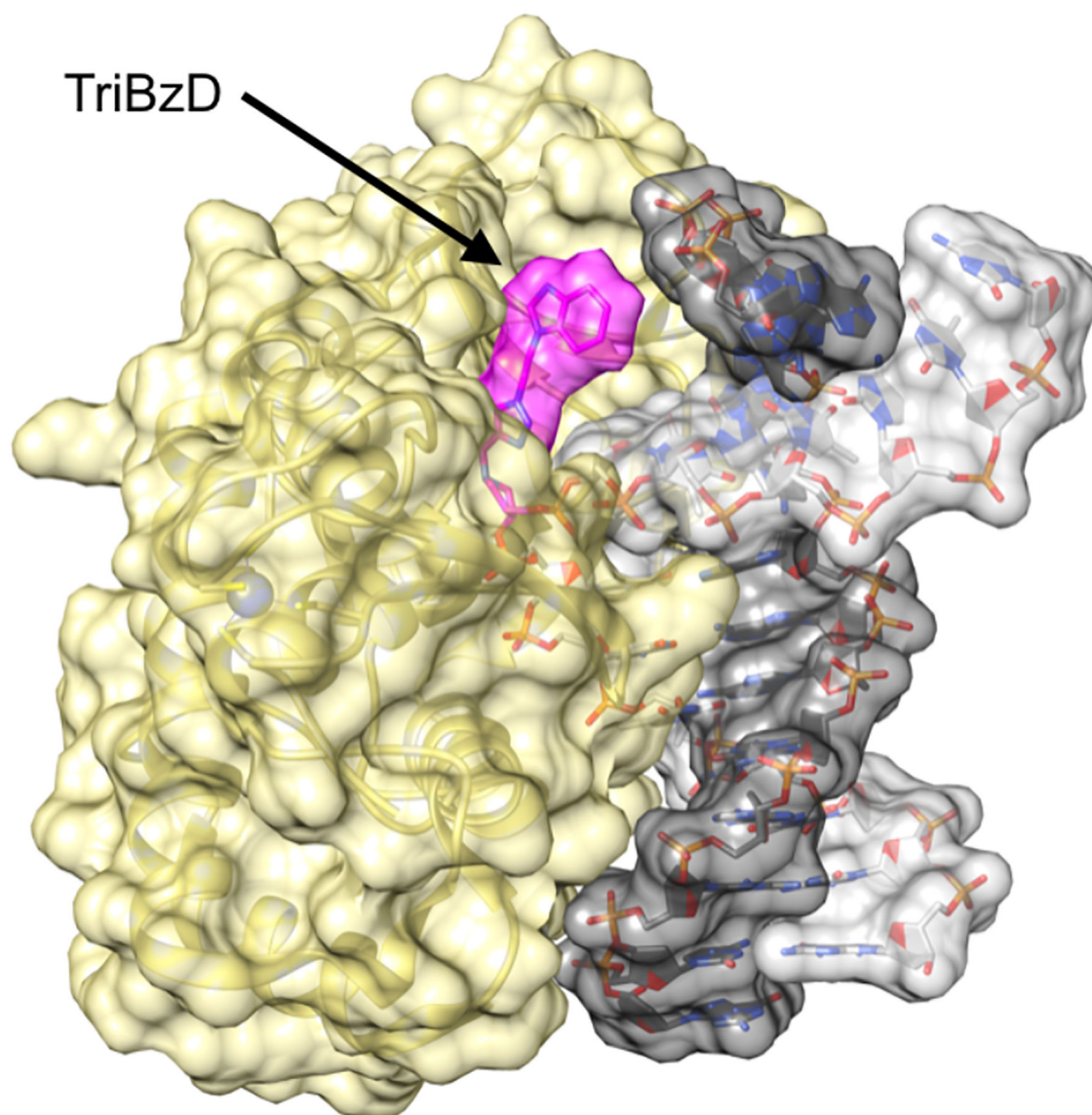


Figure 6: Model of DNA with 1N-TriBzD bound to Fpg.

DNA strands are colored dark and light grey, with the 1N-TriBzD group highlighted in magenta. The solvent accessible surface of Fpg is colored yellow. The model was constructed on the basis of the x-ray crystal structure of *LFpg* bound to DNA (PDB ID 4PCZ).⁵² The 1N-TriBzD group occupies a solvent filled space with no apparent clashes (Table S6).

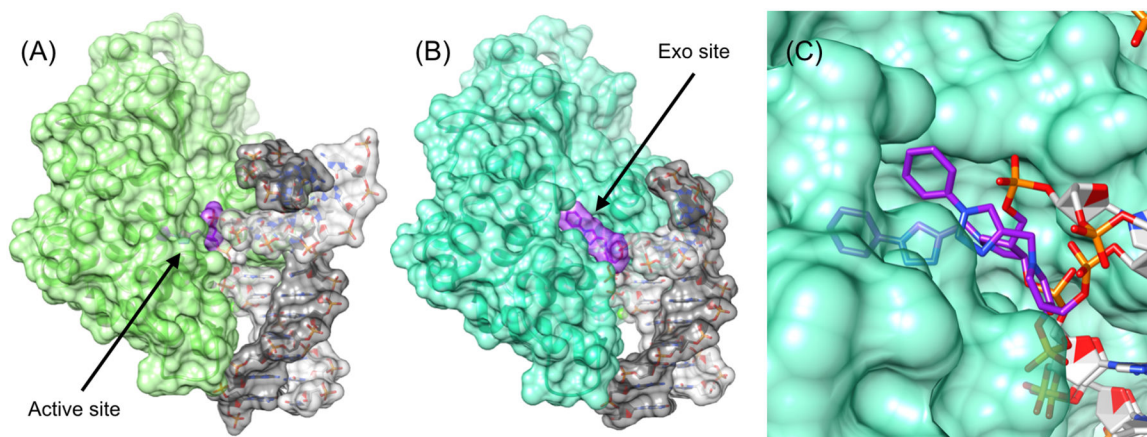
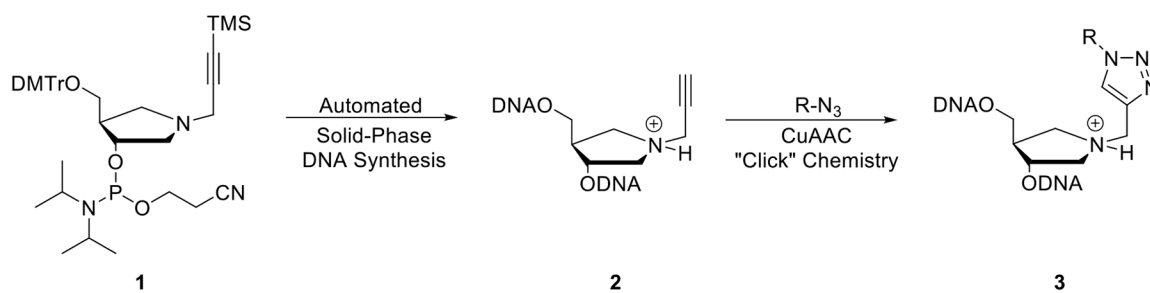


Figure 7: Structural models of DNA with 1N-TriBen bound to hOGG1.

The 1N-TriBen group fits in both the active site (A) and the *exo* site (B). Models were constructed on the basis of x-ray crystal structures of hOGG1 bound to DNA containing 8OG (A, PDB ID 1YQR) or to undamaged DNA (B, 1YQK).⁵⁵ DNA strands are colored dark and light grey, with the 1N-TriBen group highlighted in purple. The solvent accessible surface of hOGG1 is colored lime or aquamarine. (C) In this closeup view, models of 1N-TriBen were superimposed by alignment of hOGG1 coordinates (r.m.s.d. = 0.6 Å, for 281 alpha carbons). For clarity, only the surface of hOGG1 with the *exo* site occupied is shown. The Tri-Ben group fits snugly in the active site and in the *exo* site with very few steric clashes (Table S6).

**Scheme 1:**

Synthetic scheme for the development of triazole-containing pyrrolidine oligonucleotides via click chemistry.

Table 1: K_d values for hOGG1 with TS1 Mimic 30 bp duplex DNA^a

TS mimic, Analog or normal base	K_d (nM) ^b site 1, site 2 (capacity)
1N-Prop	<0.005 (76%), 40 ± 20 (19%)
1N-Tri	<0.005 (60%), 20 ± 10 (26%)
1N-TriBen	<0.005 (92%), 3 ± 2 (7%)
1N-TriBzD	<0.005 (80%), 7 ± 3 (16%)
1N-TriDiol	<0.005 (78%), 4 ± 2 (18%)
1N-TriGlcNAc	0.02 ± 0.01 (39%), 4 ± 2 (45%)
4N	<0.01 (50%), 5 ± 2 (20%) ^c
1N	<0.01 (36%), 5 ± 2 (20%) ^c
1NBn	<0.005 (72%), 32 (20%) ^c
THF	<0.005 ^c
G	>1200 ^c
FOG	2 ± 1 nM ^d

^aS30 sequence was annealed with the complement to position the TS mimic or analog opposite C in the resulting duplex (see methods).

^b K_d values determined from fitting with a two-site binding isotherm.

^cThese values were previously reported. Of note, the weaker K_d in these studies was not attributed to binding to 1N or 1NBn in ssDNA, which was found to exhibit a much higher K_d of 76 ± 12 nM, and 83 ± 15 nM, respectively.³⁶

^dFOG refers to 2'-fluoro-OG. This K_d value was previously reported in a slightly different 30-bp sequence.¹⁴